Received 23 August 2023; revised 28 October 2023; accepted 4 November 2023. Date of publication 14 November 2023; date of current version 30 January 2024.

Digital Object Identifier 10.1109/OJAP.2023.3332589

A Lightweight Spherical Generalized Luneburg Lens Antenna With Low Cross-Polarization Over a Wide Range in Azimuth and Elevation

MARAL ANSARI [1] (Member, IEEE), OSKAR ZETTERSTROM [2] (Graduate Student Member, IEEE), NELSON J. G. FONSECA [3] (Senior Member, IEEE), OSCAR QUEVEDO-TERUEL [2] (Fellow, IEEE), AND Y. JAY GUO [1] (Fellow, IEEE)

[1]Global Big Data Technologies Centre, University of Technology Sydney, Ultimo, NSW 2007, Australia

[2]Division of Electromagnetic Engineering, School of Electrical Engineering, KTH Royal Institute of Technology, 100 44 Stockholm, Sweden

[3]Antenna and Sub-Millimetre Waves Section, European Space Agency, 2200 AG Noordwijk, The Netherlands

CORRESPONDING AUTHOR: M. ANSARI (e-mail: maralansari0@gmail.com)

ABSTRACT In this paper, a novel dual-slant polarized three-dimensional (3D) periodic Luneburg lens with a diameter of 390 mm ($4.6\lambda_0$ at 3.55 GHz) is presented. Copper-plated cubes with truncated corners are placed in a body-centered cubic (BCC) lattice and held together with layers of Rohacell foam. The sizes of the cubes are varied to realize the gradient refractive index (GRIN) profile of a generalized Luneburg lens at a low cost, with a low weight and loss. The designed Luneburg lens operates from 3.3 to 3.8 GHz with a total weight of 1 kg. The quasi-isotropic response of the proposed periodic structure allows a wide angle coverage. Measured results show that the lens antenna can achieve a peak gain of 22 dBi with a scanning loss of less than 0.4 dB in a wide angular range in both the azimuth and the elevation plane. Importantly, the proposed lens antenna design achieves a cross-polarization level below peak gain of less than −19 dB at all angles for the two slant polarizations of the feed, while comparable designs report up to −11 dB at given angular directions. This high-gain multi-beam antenna with a commercially viable design is suitable for wireless communications at low microwave frequencies.

INDEX TERMS Body-centered cubic (BCC) lattice, gradient refractive index (GRIN) material, quasi-isotropic periodic structure, multi-beam Luneburg lens antenna, wide angle coverage.

I. INTRODUCTION

FUTURE generations of communication systems are expected to meet the demands for faster mobile broadband speeds, higher network capacity, and lower latency [1], [2]. In this regard, the design of antennas with dual polarization and highly directional multiple beams is of critical importance [3]. Dual-polarized antennas enable polarization diversity, and multiple beams provide spatial domain multiplexing, thus leading to increased system capacity. Different realizations of beamforming devices such as Butler matrices [4], [5], Rotman lenses [6], [7], planar and three-dimensional (3D) Luneburg lenses [8], [9], [10], [11], [12], [13] have been introduced in recent years. Planar quasi-optical beamforming structures can deliver high-gain scanned beams at low cost [14], among which, planar Luneburg lens antennas are of interest for their wide scanning range [15]. Different designs of parallel-plate cylindrical Luneburg lenses have been produced with the ability to create high directive beams in their H-plane [16], [17], [18], [19], [20]. However, such planar structures provide the communication systems with only one-dimensional (1D) steering, whilst in many practical applications, 2D beam steering is required.

Spherical Luneburg lenses are simple and attractive passive steerable antennas for wireless communication systems. The spherically symmetric structures enable two-dimensional (2D) beam steering over a wide-angular range without performance degradation [8]. The traditional method for the realization of such 3D lenses is the layered approach, where the lens is divided into a series of shells with

different refractive indexes (RIs) [21], [22]. The fabrication and assembly of several spherical shells with different RIs can be complex and costly. Alternatively, the Gradient Refractive INdex (GRIN) profile can be realized using quasi-periodic structures, resulting in Luneburg lenses with a gradual variation in their effective material properties and, consequently, low reflections within the lens.

Various quasi-periodic Luneburg lenses have been reported. For instance, Luneburg lenses based on planar layers with periodic holes drilled in dielectric slabs were reported in literature [23], [24], [25]. Recently, additive manufacturing has been used to produce Luneburg lenses operating above 10 GHz [12], [26]. This technique offers a high manufacturing resolution. However, the dielectric material and methods used in these lens designs may result in heavy and costly devices at low frequency (below 10 GHz). In [27], a low-weight, low-cost, layered structure for the construction of spherical Luneburg lenses at lower microwave frequencies was described. This method, while suited for low-weight designs, suffers from high cross-polarization at wider scan angles. A modified structure was consequently introduced in [28] where the lens layers were designed to achieve low anisotropy in the azimuth plane, at the expense of degraded performance in the elevation plane. However, the main application of the spherical Luneburg lens is to fully steer the beam in both azimuth and elevation planes, which motivates the reported research.

This paper reports a novel layered design of a periodic 3D Luneburg lens consisting of Rohacell foam with conducting inclusions placed in a novel lattice. Specifically, the periodic inclusions are arranged in a body-centred cubic (BCC) lattice, and we demonstrate that this lattice arrangement allows for a quasi-isotropic response. We use this periodic structure to design the first reported light-weight multi-beam Luneburg lens antenna with wide angular coverage in both the azimuth and elevation planes, where high cross-polarization isolation and efficiency are maintained in all angular directions. Importantly, compared with previously reported Luneburg lens antennas with the inclusions placed in simple cubic [27] or hexagonal lattices [28], the presented lens antenna maintains its attractive radiation properties for scanning in the whole angular space, demonstrating the benefits of the proposed lattice arrangement for lens designs. Specifically, the comparative analysis reported here demonstrates an improvement in cross-polarization of up to 8 dB and a reduction in side lobe level (SLL) of up to 4 dB. The use of the BCC lattice is inspired by glide-symmetric structures [29], and the observed quasi-isotropic response is similar to the previously observed response in planar glide-symmetric lenses [10], [20]. The proposed quasi-isotropic periodic structure greatly simplifies the construction of spherical lenses by virtue of planar layers instead of shells, whilst keeping the RI profile consistent. Besides, the use of foam as the supporting material makes the design light, and thus suitable for applications in bands below 10 GHz, where the weight of conventional Luneburg lenses can be

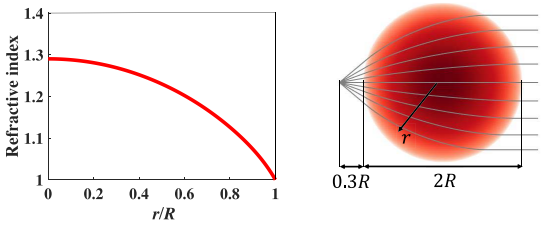

FIGURE 1. (a) Calculated RI of the lens when the focus is moved to 1.3*R* (*R* is radius of the lens, *r* is the radial position.) (b) Ray tracing of the generalized Luneburg lens.

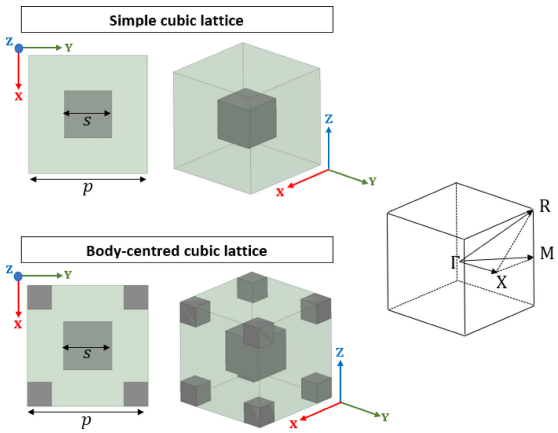

FIGURE 2. Configuration of the unit cells (left) and definition of the points of high symmetry delimiting the irreducible Brillouin zone of interest (right). The inclusions are shown in a simple cubic (SC) and in a body-centred cubic (BCC) lattice, where *p* is the period, and *s* is the side length of the inclusion.

prohibitive. It is worth to note that the volume and mass of the lens increases cubically with the radius, meaning that this is increasingly important for lower frequency and higher gain.

The high gain multi-beam lens antenna presented in this work can find applications in wireless communication systems such as fourth-generation (4G) and fifth-generation (5G) networks, specifically in the so-called frequency range 1 (FR1) corresponding to below 6 GHz frequency band allocations. The proposed design features low fabrication cost while enabling polarization diversity suitable for high capacity communication systems.

II. DESIGN OF THE LUNEBURG LENS ANTENNA

This section describes the lens antenna design. First, a quasi-isotropic structure for the realization of the effective RI profile of the lens is introduced. Then, the lens is implemented and tested with a square waveguide feed.

A. REALIZATION OF THE QUASI-PERIODIC LENS

A generalized Luneburg lens with a focal point displaced $0.3R$ from the lens surface, where R is the radius of the lens, is designed [30], [31], [32]. The corresponding RI distribution and a ray tracing representation for this lens are provided in Fig. 1. The required RI profile of the lens is

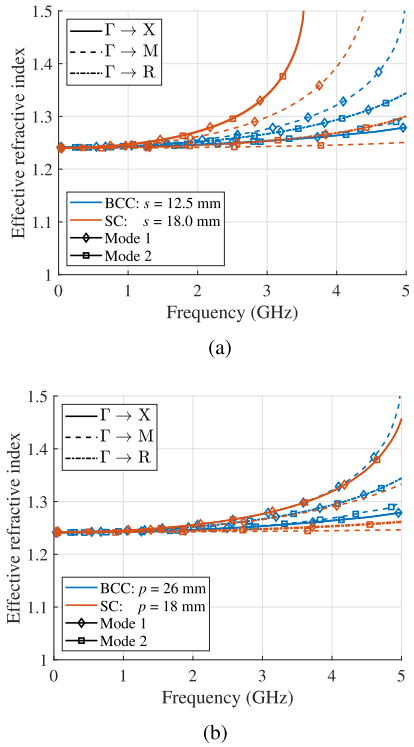

FIGURE 3. Effective refractive index of the SC and BCC lattice for propagation along the symmetry directions. (a) The structures have $p = 26$ mm and different s. (b) The structures have $s = 12.5$ mm and different p.

realized using a quasi-periodic structure, where the index of refraction is controlled by varying the size of the inclusions.

A 3D periodic quasi-isotropic BCC structure is introduced, analyzed, and its response is compared with that of a structure arranged in a simple cubic (SC) lattice. The SC structure was used in the design of the lens in [27]. It is worth noting that a dielectric BCC structure was proposed in [33] and was demonstrated to provide wide bandwidth and robust realization using additive manufacturing. The unit cells of the two structures studied here are shown in Fig. 2, where the gray color corresponds to metal and the green color corresponds to the host medium, which is assumed to be a vacuum in the simulation models. The BCC structure is inspired by previously reported 2D glide-symmetric structures [20], [34].

In a lens antenna based on these structures, the field within the lens can be expressed as a combination of these two modes with the relative amplitude between the modes depending on the local environment in the lens, the source type and source position. This means that, since the response is different for the different modes, we expect that the lens introduces some polarization impurity and phase errors, and that this performance degradation depends on the feed position.

Here, the dispersion diagrams for the two structures are obtained using the CST *eigenmode solver*. The results are shown in Fig. 3 for the propagation along $\overline{\Gamma X}$, $\overline{\Gamma M}$, and $\overline{\Gamma R}$. At the considered frequency range, the structures support

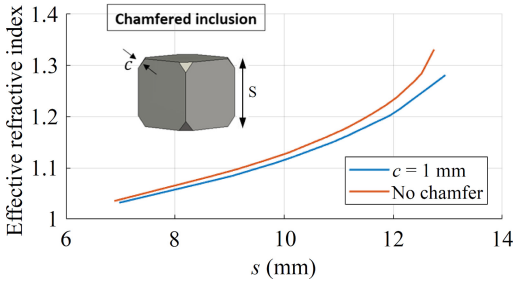

FIGURE 4. Comparison of the effective refractive index for propagation along $\Gamma \rightarrow R$ at 3.5 GHz with and without chamfered corners. The dimensions are $c = 1$ mm and $p = 26$ mm.

propagation of waves in two different modes, and these are indicated with different line markers. It is worth noting that in a lens antenna based on these structures, the field within the lens can be expressed as a combination of these two modes with the relative amplitude between the modes depending on the local environment in the lens, the source type and source position. This means that, since the response is different for the different modes, we expect that the lens introduces some polarization impurity and phase errors, and that this performance degradation depends on the feed position. With this said, we note that the structures appear identical for the two modes for propagation along $\overline{\Gamma X}$ and $\overline{\Gamma R}$, but not for $\overline{\Gamma M}$. In Fig. 3(a), the period is the same in the structures and the side length (s) is tuned so that the effective RI in the two structures at low frequencies are the same. We observe that the bandwidth of operation is significantly wider in the BCC structure. Furthermore, the response of the BCC structure for propagation along $\overline{\Gamma M}$ is more similar for the two modes, compared to the SC structure. As a result, we expect the performance to be more stable with scanning angle in a lens based on the BCC structure, compared to a lens based on the SC structure. It is noted that the bandwidth in the SC structure can be increased by reducing the period, as demonstrated in Fig. 3(b). However, we observe that the SC structure in this case still remains slightly more anisotropic and that a lens implemented with the SC structure requires a larger number of inclusions in a given volume, which can result in increased manufacturing complexity.

As required by the manufacturer to avoid issues related to tolerances, the corners of the cubic inclusions are truncated. The inclusion of chamfered corners for use in the fabricated prototype is shown in the inset of Fig. 4. Here, c is the chamfering of the corners, which is chosen to be $c = 1$ mm to comply with the manufacturing requirements. In Fig. 4, we observe that the chamfering only has a small impact on the effective refractive index. This effect is considered for the lens design.

Considering this unit cell configuration allows choosing higher periodicity with lower dispersion, the unit cell size in this design is chosen to be equal to $26 \times 26 \times 26\,\text{mm}^3$, corresponding to $p = 26$ mm, which is $0.3\lambda_0$ at mid-band frequency. The side length of the cubic inclusions with 1 mm

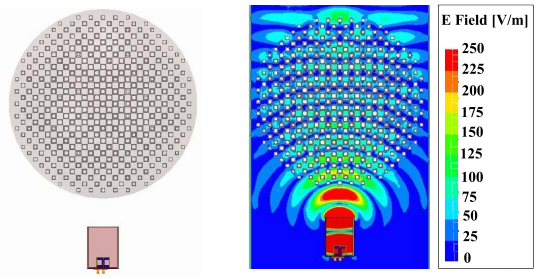

FIGURE 5. Lens antenna in full-wave simulator. (a) The lens antenna structure. (b) E-field distribution at mid band frequency. The lens radius is 195 mm ($2.3\lambda_0$ at 3.55 GHz).

TABLE 1. Radial distribution of inclusions versus side length.

Side length, s	Radial range	Quantity
7.5 mm	196-199.5 mm	930
9 mm	191-196 mm	560
10 mm	178-190 mm	470
11 mm	166-178 mm	564
11.5 mm	152-166 mm	518
12 mm	131-152 mm	418
12.5 mm	111-131 mm	292
13 mm	0-110 mm	15

chamfering varies from 7.5 mm to 13 mm in minimum steps of 0.5 mm to approximate the effective RI distribution as required for this lens design. Eight different sizes of inclusions are used and their radial distribution is detailed in Table 1. From previous works on discretized Luneburg lenses, this is considered to provide sufficient sampling of the continuous RI profile [35]. Note that the inclusions at the center of the lens require a cube with a side of half-a-period, hence the benefit of using chamfered corners to avoid issues related to manufacturing tolerances.

B. LENS ANTENNA DESIGN

A square waveguide feed excited by a PCB crossed-dipole [27] is used to investigate the dual-slant polarized performance of the lens. The feed is placed at a distance of $0.3R$ from the lens surface. The simulated model of the lens antenna system and E-field distribution is shown in Fig. 5. The simulated normalized radiation patterns of the lens antenna at mid-band frequency (3.55 GHz) are compared with the ones in [27], [28] to demonstrate the superior performance of this new design. The results are shown in Fig. 6. Comparison of the plots shows that the proposed lens antenna offers the most stable performance across the analysed scanning range. For the lens with cubic lattice and cubic inclusions [27], high SLL and cross polarization discrimination (XPD) are observed at wider scan angles ($\pm 45°$ for this case) where defocusing causes larger phase error on the lens aperture. The modified design of hexagonal lattice with cylindrical inclusions introduced in [28] improves the scanning performance in the azimuth plane and delivers

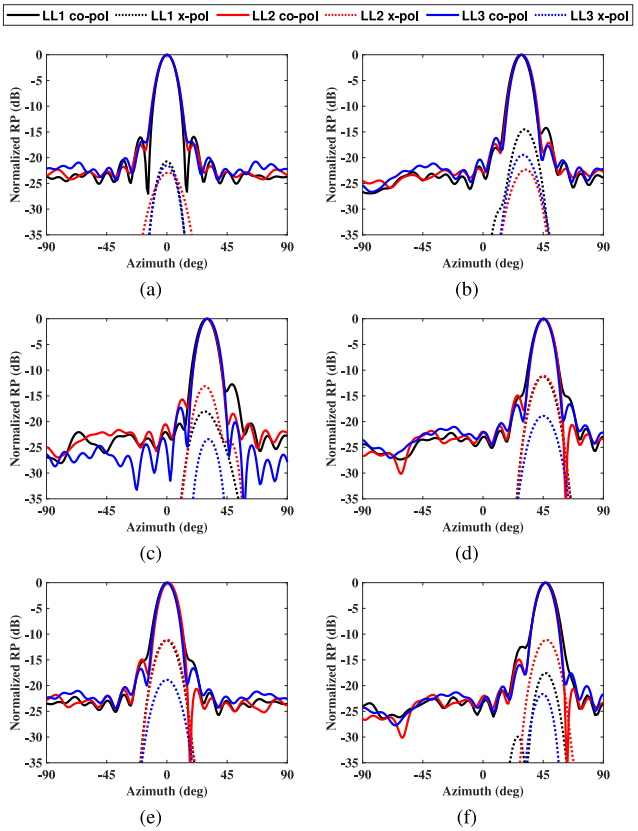

FIGURE 6. Comparison of the simulated azimuth radiation patterns (RP) of this work (LL3) with the ones in [27] (LL1) and [28] (LL2) at 3.55 GHz at (a) 0° Az 0° El (b) 30° Az 0° El (c) 30° Az 30° El (d) 45° Az 0° El (e) 0° Az 45° El (f) 45° Az 45° El.

the best figures for scanning in the azimuth plane. However, when it comes to the elevation scanning, the SLL and XPD becomes the worst, mainly because this design in not symmetric along the elevation plane. On the other hand, with the proposed lens design using BCC unit cells, the patterns repeat every 45°. This is due to the symmetries in the unit cell layout as shown in Fig. 5, which preserve the symmetries already discussed at unit cell level in Section II-A. As a consequence, the lens is invariant upon rotation of 90° around any of the main axes. Further combined with reflection symmetries, the results reported here can be reduced without lack of generality to a scanning range of [0° 45°] in both azimuth and elevation. In this lens antenna, the SLL and XPD stay below −15 dB and −19 dB, respectively, across all the angles. The gain, beamwidth, and aperture efficiency are similar to the other two lenses. The performance in SLL, and more generally beam shape, provide a good indication of the focusing characteristics of the lenses, while the XPD is a good indicator of the polarization sensitivity. The results reported demonstrate the improvement achieved using quasi-isotropic unit cells.

III. EXPERIMENTAL RESULTS

In this section, the fabrication process of the lens antenna is described. The prototype lens antenna is measured in

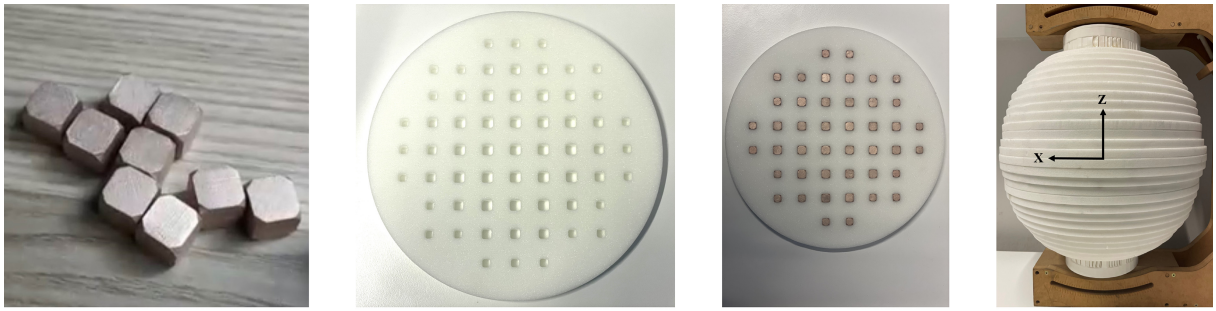

FIGURE 7. Lens construction. (a) Copper plated foams inclusions. (b) Foam layer. (c) Inclusions placed in a layer. (d) Prototype of the complete spherical Luneburg lens, including the reference coordinate system in which the azimuth and elevation angles are defined.

an anechoic chamber. Finally, the simulation and measured results are compared with the state-of-the art Luneburg lenses.

A. LENS FABRICATION AND TEST

The presented Luneburg lens antenna has been fabricated and tested. The lens has a diameter of 390 mm in the vertical direction and a diameter of 400 mm in the horizontal to ensure that inclusions are not too close to the edge. It comprises 30 cylindrical layers of Rohacell (a lightweight structural foam with a dielectric constant close to that of air) and a thickness of 13 mm for each layer. Through square holes were cut from foam layers to accommodate the inclusions. The layers are stacked up in the vertical direction to form the complete sphere. A total of 3479 inclusions are required for the lens design, as detailed in Table 1. Two sets of inclusions were fabricated. The first three big sizes were made by 3D printed plastic material coated with copper. The corners are also chamfered as shown in Fig. 7 (a). The rest of the inclusions were cut from foam and electrolytically plated with copper. The reason for such a choice is to avoid contact of big inclusions, requiring more precise manufacturing, while smaller inclusions are less sensitive and can be manufactured using cheaper processes. Next, the inclusions are placed inside the layers' holes. One of the foam layers, inclusions, and a layer of lens are shown in Fig. 7. The complete lens prototype weights almost 1 kg, which is very lightweight for a lens of this size. Since the weight of the system scales cubically with the radius of the lens, the density of the material used for implementation must be minimized. A similar lens implemented with dielectric thermoplastic or polystyrene, having a density typically around 1 g/cm^3, would weight approximately 20 kg, which is significantly heavier than the proposed design. This estimate of the weight accounts for the filling factor varying with the refractive index profile. As an example, the additively manufactured half-Gutman lens in [33] weights 77.4 g for a radius of 4 cm, corresponding to an average density of 0.3 g/cm^3, which would scale up to 19.4 kg for a full lens with a radius of 20 cm similar to the one considered in this work.

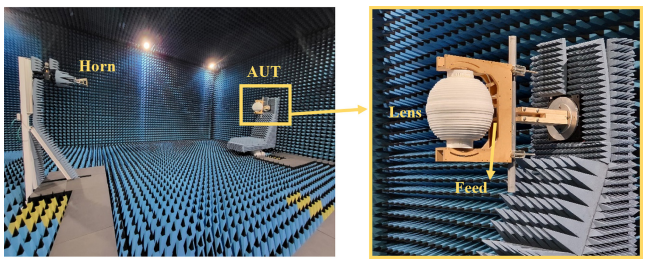

FIGURE 8. Lens antenna prototype in the anechoic chamber. The azimuth is measured by rotating the lens about its axis. The elevation scanning is measured by rotating the feed along the lens elevation.

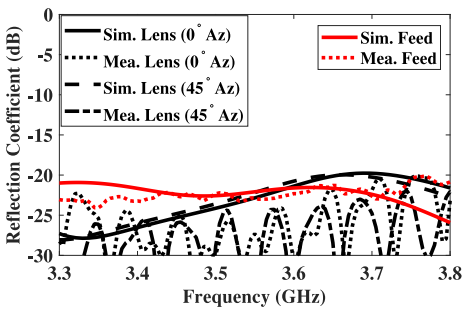

FIGURE 9. Simulated and measured reflection coefficients of the feed and of the lens with feed.

Far-field measurements of the lens antenna were made in the NSI anechoic chamber at UTS Techlab, NSW, Australia. To hold the lens on the positioner, a wooden fixture was constructed that also supports the feed at a distance of 60 mm ($0.3R$) from the lens surface. It allows to rotate the feed at different elevation angles, while the azimuth scanning performance is tested by rotating the lens along its polar axis. The lens antenna measurement setup is shown in Fig. 8.

B. SIMULATION AND MEASUREMENT RESULTS

In this section, the simulated and measured results of the lens antenna are compared. First, an Agilent Network Analyzer N5225A has been used to measure the reflection coefficients of the feed alone and with the lens antenna. These results are given in Fig. 9. The feed rotation along the lens surface does not affect significantly the reflection coefficient of the

TABLE 2. Comparison with other reported spherical Luneburg lens antennas.

Ref.	Realization	Feed Type	Frequency Band (GHz)	Scan Angle Az/El (deg)	Gain (dBi)	HPBW Az/El (deg)	SLL Az/El (dB)	Radiation Efficiency (%)	Aperture Efficiency (%)	XPD at wide angles (dB)	Pol.
[24]	Perforated slices	Open-ended waveguide	12-18	±75 (Azimuth only)	23.1-25.7	11/14	-9/-22.8	80	47-93	N.G.	LP
[26]	3D Printing (cubes)	Open-ended waveguide	8-12	N.G.	17.3-20.3	13/19	-20/-25	N.G.	47-53	N.G.	LP
[36]	Randomely distributed conductive fibres	Horn	3-6	Full range	23-28.5	5.2-10.6	-21 (boresight)	N.G.	50-56.2	N.G.	LP (VP)
[27]	Conductive cubes in cubic grid	Open-ended waveguide	3.3-3.8	±60/ ± 60	21.9-23.4	13/14.5	-12/-11	91	75-85	-11	Dual-LP (Slant)
[28]	Conductive cylindrical in hexagonal grid	Open-ended waveguide	3.3-3.8	±60/ ± 30	21.3-22.8	12.4/13.9	-16/-12	97	71-84	-11	Dual-LP (Slant)
This work	Conductive BCC in cubic grid	Open-ended waveguide	3.3-3.8	Full range	21.2-23.3	13/14.2	-15/-15	95	71.5-89	-19	Dual-LP (Slant)

* Az/El:Azimuth/Elevation; HPBW: half-power beamwidth; LP: linear polarization; N.G.:not given; SLL: sidelobe level; XPD: cross polarization discrimination.

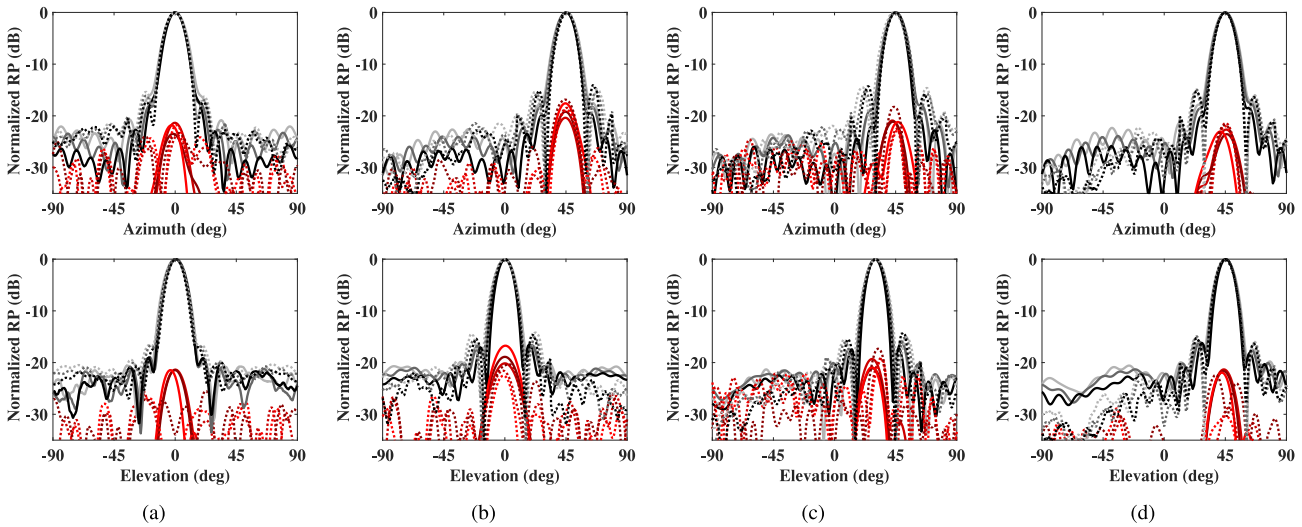

FIGURE 10. Simulated (solid line) and measured (dash line) normalized co-polar and cross-polar radiation patterns of the lens antenna at +45° polarization for the beams at (a) 0° Az 0° El. (b) 45° Az 0° El. (c) 45° Az 30° El. (d) 45° Az 45° El. Frequency superimposed: 3.3 GHz, 3.5 GHz, 3.8 GHz. (Note: The lens has 4-fold symmetry, so the patterns at 0° Az 45° El are similar to the ones at 45° Az 0° El.)

lens antenna system, so this figure is only shown for the feed at 0° and 45° azimuth. The reflection coefficient of the feed with the lens is less than −20 dB across the band. The measured port-to-port isolation is below −30 dB and is not reported here for brevity. Good agreement between the simulated and measured results is observed. Then, radiation property of the proposed 3D Luneburg is investigated in detail.

The simulated and measured radiation patterns of the lens antenna at normal incidence and some of the selected angles at three different frequencies across the band (3.3, 3.55, 3.8 GHz) for one of the slant polarizations are shown in Fig. 10. Since the lens patterns repeat after 45° in azimuth and elevation as a direct consequence of the symmetries discussed in Section II-B, we only show the patterns up to this angle, and the reported results cover the worst case. The simulated and measured results agree well. Although the beam shape and beamwidth is stable across the band at different angles, higher SLL is observed in the measured results, which is attributed mostly to the test fixture. Fig. 11 compares the simulated and measured gain with the maximum ideal directivity, which is evaluated based on a uniform illumination of an aperture with area A (i.e., $D_{\max} = 4\pi A/\lambda^2$), where A is the cross section area

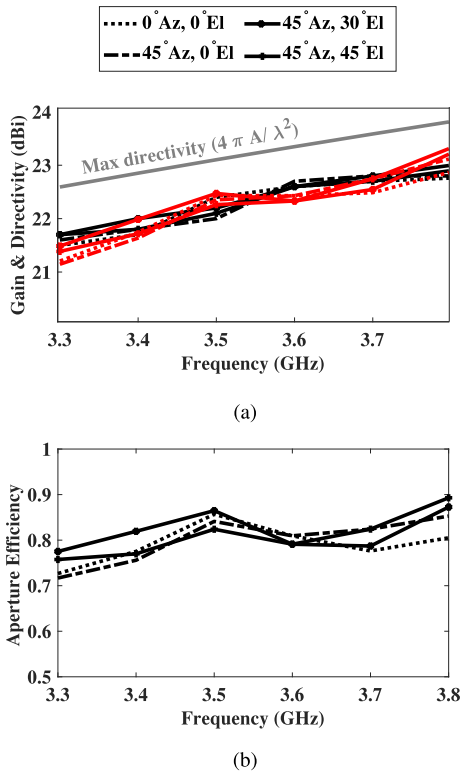

FIGURE 11. (a) Simulated (black lines) and measured (red lines) realized gain, and maximum ideal directivity. (b) Aperture efficiency versus gain.

of the lens. The plots show that the realized gain varies from 21.15 to 23.3 dBi at all angles with a scan loss of less than 0.4 dB in all cases. Comparison of the simulated and measured realized gain and maximum ideal directivity shows the aperture illumination efficiency is better than 70% across the band from 3.3 to 3.8 GHz, while the radiation efficiency stays better than 95%. These plots are shown in Fig. 11 (b). It is to be noted that much of the losses are due to spillover from the feed, corresponding to the radiated power not being intercepting by the lens. This demonstrates the very low loss nature of the lens material resulting in a very high efficiency.

C. COMPARISON AND DISCUSSION

The Luneburg lenses are primarily used in high frequencies and mm-wave applications. A direct comparison with the mm-wave designs is difficult because the technique suitable for such methods is not practical for low microwave frequencies. In Table 2, the performance of the Luneburg lens antenna reported in this work is compared with the state-of-the-art lens antennas. The perforated slices and 3D printing techniques used in [24], [26] are not applicable for the fabrication of the very large lens antennas at lower microwave frequencies. Such material has high density making the design not viable for commercial use. In [37], concentric spherical shells comprising lightweight foam with embedded randomly conductive wires are used, which overcomes the weight problem. From a construction point of view, however, maintaining the consistency of the profile within each shell is difficult. The last three entries correspond to the layered lens designs at lower microwave frequencies, where all the designs use the same feed and have the same size and operating frequency within the band 3.3 GHz to 3.8 GHz, with the possibility to extend the bandwidth as described in [28]. Comparisons of the radiation pattern of these lenses as displayed in Fig. 6 show that all three lenses perform the same at boresight, while they differ in scanning performance. The design in [27] shows variation in SLL, and cross-polarization level with azimuth scanning. Although the hexagonal lattice used in [28] reduces the anisotropy in the azimuth plane and has lower fabrication complexity thanks to cylindrical inclusions and reduced number of layers, the performance deteriorates at larger elevation angles. The quasi-isotropic periodic structure in this work allows the best scanning performance among all other reported works, making the design suitable for full coverage high gain multi-beam steerable antennas.

IV. CONCLUSION

A multi-beam high-gain antenna has been presented using a 3D generalized Luneburg lens fed by a dual-polarized square waveguide operating at sub-6GHz bands. The GRIN material is realized by placing conductive inclusions in a BCC lattice supported by Rohacell foam layers. The design shows low loss and is highly efficient, and produces directive beams in the whole space without any notable performance variation when fed from different positions. This wide angle scanning capability is a consequence of the symmetry of the BCC lattice, which can be used to overcome the scanning limitations in previously reported lens antennas using similar inserts [27], [28]. The concept is demonstrated by an experimental prototype and the simulated and experimental results agree well. The presented work is a suitable high gain beam steering and multi-beam antenna for use in commercial microwave communications systems such as 4G, 5G sub-6GHz band, GPS, WiMax, etc.

ACKNOWLEDGMENT

The authors would like to thank Dr. Wei Lin, Hong Kong Polytechnic University, for helping with the manufacturing of the prototype, Dr. Majid Amiri, University of Technology Sydney, for helping with the testing of the prototype antenna at UTS Techlab NSI antenna chamber, and Prof. Bevan Jones, Vecta Pty Ltd. for the valuable discussions.

REFERENCES

[1] J. G. Andrews et al., "What will 5G be?" *IEEE J. Sel. Areas Commun.*, vol. 32, no. 6, pp. 1065–1082, Jun. 2014.
[2] A. Gupta and R. K. Jha, "A survey of 5G network: Architecture and emerging technologies," *IEEE Access*, vol. 3, pp. 1206–1232, 2015.
[3] T. S. Rappaport et al., "Millimeter wave mobile communications for 5G cellular: It will work!" *IEEE Access*, vol. 1, pp. 335–349, 2013.
[4] A. A. M. Ali, N. J. G. Fonseca, F. Coccetti, and H. Aubert, "Design and implementation of two-layer compact wideband Butler matrices in SIW technology for Ku-band applications," *IEEE Trans. Antennas Propag.*, vol. 59, no. 2, pp. 503–512, Feb. 2011.

[5] J.-W. Lian, Y.-L. Ban, Q.-L. Yang, B. Fu, Z.-F. Yu, and L.-K. Sun, "Planar millimeter-wave 2-D beam-scanning multibeam array antenna fed by compact SIW beam-forming network," *IEEE Trans. Antennas Propag.*, vol. 66, no. 3, pp. 1299–1310, Mar. 2018.
[6] Y. J. Cheng et al., "Substrate integrated waveguide (SIW) Rotman lens and its Ka-band multibeam array antenna applications," *IEEE Trans. Antennas Propag.*, vol. 56, no. 8, pp. 2504–2513, Aug. 2008.
[7] J.-W. Lian, Y.-L. Ban, H. Zhu, and Y. Guo, "Reduced-sidelobe multibeam array antenna based on SIW Rotman lens," *IEEE Antennas Wireless Propag. Lett.*, vol. 19, pp. 188–192, 2020.
[8] R. K. Luneburg, *Mathematical Theory of Optics*. Berkeley, CA, USA: Univ. California Press, 1964.
[9] C. Pfeiffer and A. Grbic, "A printed, broadband Luneburg lens antenna," *IEEE Trans. Antennas Propag.*, vol. 58, no. 9, pp. 3055–3059, Sep. 2010.
[10] O. Quevedo-Teruel, M. Ebrahimpouri, and M. Ng Mou Kehn, "Ultrawideband metasurface lenses based on off-shifted opposite layers," *IEEE Antennas Wireless Propag. Lett.*, vol. 15, pp. 484–487, 2016.
[11] N. J. G. Fonseca, Q. Liao, and O. Quevedo-Teruel, "Equivalent planar lens ray-tracing model to design modulated geodesic lenses using non-Euclidean transformation optics," *IEEE Trans. Antennas Propag.*, vol. 68, no. 5, pp. 3410–3422, May 2020.
[12] Y. Li, L. Ge, M. Chen, Z. Zhang, Z. Li, and J. Wang, "Multibeam 3-D-printed Luneburg lens fed by magnetoelectric dipole antennas for millimeter-wave MIMO applications," *IEEE Trans. Antennas Propag.*, vol. 67, no. 5, pp. 2923–2933, May 2019.
[13] H. Saghlatoon, M. M. Honari, S. Aslanzadeh, and R. Mirzavand, "Electrically-small Luneburg lens for antenna gain enhancement using new 3D printing filling technique," *AEU-Int. J. Electron. Commun.*, vol. 124, Sep. 2020, Art. no. 153352.
[14] Y. J. Guo, M. Ansari, R. W. Ziolkowski, and N. J. G. Fonseca, "Quasi-optical multi-beam antenna technologies for B5G and 6G mmWave and THz networks: A review," *IEEE Open J. Antennas Propag.*, vol. 2, pp. 807–830, 2021.
[15] O. Quevedo-Teruel, M. Ebrahimpouri, and F. Ghasemifard, "Lens antennas for 5G communications systems," *IEEE Commun. Mag.*, vol. 56, no. 7, pp. 36–41, Jul. 2018.
[16] H.-T. Chou and Z.-D. Yan, "Parallel-plate Luneburg lens antenna for broadband multibeam radiation at millimeter-wave frequencies with design optimization," *IEEE Trans. Antennas Propag.*, vol. 66, no. 11, pp. 5794–5804, Nov. 2018.
[17] C. Hua, X. Wu, N. Yang, and W. Wu, "Air-filled parallel-plate cylindrical modified Luneberg lens antenna for multiple-beam scanning at millimeter-wave frequencies," *IEEE Trans. Microw. Theory Techn.*, vol. 61, no. 1, pp. 436–443, Jan. 2013.
[18] A. B. Numan, J.-F. Frigon, and J.-J. Laurin, "Printed *W*-band multibeam antenna with Luneburg lens-based beamforming network," *IEEE Trans. Antennas Propag.*, vol. 66, no. 10, pp. 5614–5619, Oct. 2018.
[19] C. Wang, J. Wu, and Y.-X. Guo, "A 3D-printed wideband circularly polarized parallel-plate Luneburg lens antenna," *IEEE Trans. Antennas Propag.*, vol. 68, no. 6, pp. 4944–4949, Jun. 2020.
[20] J.-M. Poyanco, O. Zetterstrom, P. Castillo-Tapia, N. J. G. Fonseca, F. Pizarro, and O. Quevedo-Teruel, "Two-dimensional glide-symmetric dielectric structures for planar graded-index lens antennas," *IEEE Antennas Wireless Propag. Lett.*, vol. 20, pp. 2171–2175, 2021.
[21] A. Boriskin, A. Vorobyov, and R. Sauleau, "Two-shell radially symmetric dielectric lenses as low-cost analogs of the Luneburg lens," *IEEE Trans. Antennas Propag.*, vol. 59, no. 8, pp. 3089–3093, Aug. 2011.
[22] B. Fuchs, L. Le Coq, O. Lafond, S. Rondineau, and M. Himdi, "Design optimization of multishell Luneburg lenses," *IEEE Trans. Antennas Propag.*, vol. 55, no. 2, pp. 283–289, Feb. 2007.
[23] S. Rondineau, M. Himdi, and J. Sorieux, "A sliced spherical Luneburg lens," *IEEE Antennas Wireless Propag. Lett.*, vol. 2, pp. 163–166, 2003.
[24] H. F. Ma, B. G. Cai, T. X. Zhang, Y. Yang, W. X. Jiang, and T. J. Cui, "Three-dimensional gradient-index materials and their applications in microwave lens antennas," *IEEE Trans. Antennas Propag.*, vol. 61, no. 5, pp. 2561–2569, May 2013.
[25] H. F. Ma and T. J. Cui, "Three-dimensional broadband and broad-angle transformation-optics lens," *Nat. Commun.*, vol. 1, no. 1, pp. 1–7, 2010.
[26] M. Liang, W.-R. Ng, K. Chang, K. Gbele, M. E. Gehm, and H. Xin, "A 3-D Luneburg lens antenna fabricated by polymer jetting rapid prototyping," *IEEE Trans. Antennas Propag.*, vol. 62, no. 4, pp. 1799–1807, Apr. 2014.
[27] M. Ansari, B. Jones, H. Zhu, N. Shariati, and Y. J. Guo, "A highly efficient spherical Luneburg lens for low microwave frequencies realized with a metal-based artificial medium," *IEEE Trans. Antennas Propag.*, vol. 69, no. 7, pp. 3758–3770, Jul. 2021.
[28] M. Ansari, B. Jones, and Y. J. Guo, "Spherical Luneburg lens of layered structure with low anisotropy and low cost," *IEEE Trans. Antennas Propag.*, vol. 70, no. 6, pp. 4307–4318, Jun. 2022.
[29] O. Quevedo-Teruel, Q. Chen, F. Mesa, N. J. G. Fonseca, and G. Valerio, "On the benefits of glide symmetries for microwave devices," *IEEE J. Microw.*, vol. 1, no. 1, pp. 457–469, Jan. 2021.
[30] S. P. Morgan, "General solution of the Luneberg lens problem," *J. Appl. Phys.*, vol. 29, no. 9, pp. 1358–1368, Feb. 1958.
[31] W. Southwell, "Index profiles for generalized Luneburg lenses and their use in planar optical waveguides," *J. Opt. Soc. Am.*, vol. 67, no. 8, pp. 1010–1014, 1977.
[32] J. Sochacki, "Exact analytical solution of the generalized Luneburg lens problem," *J. Opt. Soc. Am.*, vol. 73, no. 6, pp. 789–795, 1983.
[33] O. Zetterstrom, N. J. G. Fonseca, and O. Quevedo-Teruel, "Additively manufactured half-Gutman lens antenna for mobile satellite communications," *IEEE Antennas Wireless Propag. Lett.*, vol. 22, pp. 759–763, 2023.
[34] O. Zetterstrom, N. J. G. Fonseca, and O. Quevedo-Teruel, "Compact half-Luneburg lens antenna based on a glide-symmetric dielectric structure," *IEEE Antennas Wireless Propag. Lett.*, vol. 21, pp. 2283–2287, 2022.
[35] A. N. Korotkov, S. N. Shabunin, and V. A. Chechetkin, "The cylindrical Luneburg lens discretization influence on its radiation parameters," in *Proc. Int. Multi-Conf. Eng., Comput. Inf. Sci. (SIBIRCON)*, 2017, pp. 394–398.
[36] R. Ryazantsev, A. Alexandrin, Y. Salomatov, and M. Sugak, "Artificial dielectric spherical Luneberg lens," in *Russian Physics Journal*. Tomsk, Russia: Tomsk State Univ. publ., 2010, pp. 70–72.
[37] S. Matitsine, "Artificial dielectric material and method of manufacturing the same," U.S. Patent 8 518 537, Aug 2013.

MARAL ANSARI (Member, IEEE) received the M.S. degree (Hons.) in electrical and communication engineering from Tabriz University, Tabriz, Iran, in 2015, and the Ph.D. degree from the University of Technology Sydney, Ultimo, NSW, Australia, in 2022. She is currently a Research Engineer with the Space and Astronomy Group, CSIRO, Marsfield, NSW, Australia. Her current research interests include multibeam antenna arrays, lens antennas, mmWave beam scanning, and beamforming networks.

OSKAR ZETTERSTROM (Graduate Student Member, IEEE) received the B.Sc., M.Sc., and Lic. degrees in electrical and electromagnetic engineering from the KTH Royal Institute of Technology, Stockholm, Sweden, in 2016, 2019, and 2021, respectively, where he is currently pursuing the Ph.D. degree in antennas and electromagnetics with the Division of Electromagnetic Engineering. He has authored or coauthored over 70 peer-reviewed journal and conference papers. His research has been focused on transformation optics, lens antennas, metamaterials possessing higher symmetries, and leaky-wave antennas. He has been awarded the 1st price in the Student Design Competition at APS/URSI 2016, the Best Student Paper Award at URSI Spain 2020, and the Best Antenna Technology Paper Award at EuCAP 2022 for his works. He is also a member of the EurAAP Working Group for Early Careers in Antennas and Propagation, for which he is responsible for the mentorship programme.

NELSON J. G. FONSECA (Senior Member, IEEE) received the M.Eng. degree in electrical engineering from the Ecole Nationale Supérieure d'Electrotechnique, Electronique, Informatique, Hydraulique et Télécommunications, Toulouse, France, in 2003, the M.Sc. degree in electrical engineering from the Ecole Polytechnique de Montreal, Montreal, QC, Canada, in 2003, and the Ph.D. degree in electrical engineering from the Institut National Polytechnique de Toulouse—Université de Toulouse, France, in 2010.

He currently works as an Antenna Engineer with the Antennas and Sub-Millimetre Waves Section, European Space Agency (ESA), Noordwijk, The Netherlands. Since November 2020, he also holds an Honorary Appointment as a Professional Fellow with the University of Technology Sydney, Australia. He has authored or coauthored more than 300 papers in peer-reviewed journals and conferences, and has over 50 patents issued or pending. His research interests include multiple beam antennas for space missions, beam-former theory and design, ground terminal antennas, and novel manufacturing techniques.

Dr. Fonseca is currently serving as an Associate Editor for the IEEE TRANSACTIONS ON ANTENNAS AND PROPAGATION and the *IET Microwaves, Antennas and Propagation* and a Topic Editor for the IEEE JOURNAL OF MICROWAVES. He is the Chair of the IEEE MTT-S Technical Committee 29 (TC-29) on Microwave Aerospace Systems and was the Guest Editor of two Focused Issues on Aerospace Applications for the *IEEE Microwave Magazine* in October 2022 and in February 2023. He has been a Board Member of the European School of Antennas and Propagation (ESoA) since January 2019 and is also serving as the Coordinator of the ESA/ESoA course on Antennas for Space Applications. He is the elected EurAAP Regional Delegate representing Benelux for the term 2021–2023.

OSCAR QUEVEDO-TERUEL (Fellow, IEEE) received the Telecommunication Engineering and Ph.D. degrees from the Carlos III University of Madrid, Spain, in 2005 and 2010, respectively.

From 2010 to 2011, he was a Research Fellow with the Department of Theoretical Physics of Condensed Matter, Universidad Autonoma de Madrid and went on to continue his postdoctoral research with the Queen Mary University of London from 2011 to 2013. In 2014, he joined the Division of Electromagnetic Engineering and Fusion Science, School of Electrical Engineering and Computer Science, KTH Royal Institute of Technology, Stockholm, Sweden, where he is a Professor and the Director of the Master Programme in Electromagnetics Fusion and Space Engineering. He has made scientific contributions to higher symmetries, transformation optics, lens antennas, metasurfaces, and high-impedance surfaces. He is the coauthor of more than 140 papers in international journals and 240 at international conferences.

Prof. Quevedo-Teruel was an Associate Editor of the IEEE TRANSACTIONS ON ANTENNAS AND PROPAGATION from 2018 to 2022 and has been a Track Editor of the IEEE TRANSACTIONS ON ANTENNAS AND PROPAGATION since 2022. He has also been the Founder and the Editor-in-Chief of the *Reviews of Electromagnetics* (EurAAP) since 2020. He was the EurAAP delegate for Sweden, Norway, and Iceland from 2018 to 2020 and he has been a member of the EurAAP Board of Directors since January 2021. Since January 2022, he has been the Vice-Chair of EurAAP. He was a Distinguished Lecturer of the IEEE Antennas and Propagation Society from 2019 to 2021. He has been the Chair of the IEEE APS Educational Initiatives Programme since 2020.

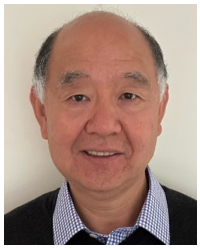

Y. JAY GUO (Fellow, IEEE) received the bachelor's and master's degrees from Xidian University, China, in 1982 and 1984, respectively, and the Ph.D. degree from Xi'an Jiaotong University, China, in 1987.

He is a Distinguished Professor and the Director of the Global Big Data Technologies Centre, University of Technology Sydney (UTS), Australia. He is the Founding Technical Director of the New South Wales Connectivity Innovation Network. Prior to joining UTS in 2014, he served as the Director of CSIRO for over nine years. Before joining CSIRO, he held various senior technology leadership positions in Fujitsu; Siemens; and NEC, U.K. He has published six books and over 700 research papers, and he holds 26 international patents. His current research interests include 6G antennas, mm-wave and THz communications and sensing systems, as well as big data technologies.

Dr. Guo has won a number of the most prestigious Australian national awards, including the Engineering Excellence Awards in 2007 and 2012 and CSIRO Chairman's Medal in 2007 and 2012. He was named one of the most influential engineers in Australia in 2014 and 2015, and Australia's Research Field Leader in Electromagnetism by the Australian Research Report for four consecutive years since 2020. Together with his students and postdocs, he has won numerous best paper awards. In 2023, he received the prestigious IEEE APS Sergei A. Schelkunoff Transactions Paper Prize Award. He has chaired numerous international conferences and served as a guest editor for a number of IEEE publications. He was the Chair of International Steering Committee, International Symposium on Antennas and Propagation from 2019 to 2021. He has been the International Advisory Committee Chair of IEEE VTC2017, the General Chair of ISAP2022, ISAP2015, iWAT2014, and WPMC'2014, and the TPC Chair of 2010 IEEE WCNC, and 2012 and 2007 IEEE ISCIT. He served as a Guest Editor of special issues on "Low-Cost Wide-Angle Beam Scanning Antennas", "Antennas for Satellite Communications," and "Antennas and Propagation Aspects of 60–90 GHz Wireless Communications," all in IEEE TRANSACTIONS ON ANTENNAS AND PROPAGATION, Special Issue on "Communications Challenges and Dynamics for Unmanned Autonomous Vehicles," IEEE JOURNAL ON SELECTED AREAS IN COMMUNICATIONS, and Special Issue on "5G for Mission Critical Machine Communications", *IEEE Network Magazine*. He was a member of the College of Experts of Australian Research Council from 2016 to 2018. He is a Fellow of the Australian Academy of Engineering and Technology.